Indian Journal of Pure & Applied Physics
Vol. 62, June 2024, pp. 429-440
DOI: 10.56042/ijpap.v62i6.8667

Investigating Structure and Physical Properties of Chromium Oxide Doped Bismuth Borate Glasses

Deepika Maan, Deepika Nain & Meenakshi*

Department of Physics, Baba Masthnath University Rohtak, Rohtak, Haryana 124 001, India

Received 9 February 2024; accepted 5 March 2024

The glasses, composed of multiple components, contain chromium oxide $x.Cr_2O_3.(70\text{-}x)B_2O_3.18Bi_2O_3.12Na_2O$, where x varies (x=0, x=0.15, x=0.25, x=0.35, x=0.50 mol %), synthesized using the melt-quench method. The amorphous nature of the synthesized samples was confirmed using X-ray diffraction (XRD). We observed that an increase in Cr_2O_3 content resulted in a rise in the density (ρ) of the glasses, ranging from 3.88 g/cm^3 to 4.009 g/cm^3. Notably, the molar volume displays behaviour opposite to the density trends. The oxygen packing density (OPD) exhibited augmentation with elevated chromium oxide concentrations, implying a more compact and tightly packed glass structure. Fourier transform infrared (FTIR) spectroscopic data show distinct features of the synthesized glass samples corresponding to chromium oxide content. The FTIR spectra display vibrations of metal cations and Cr^{3+} at around 530 cm^{-1}, and a band at approximately 1150 cm^{-1}, attributed to the B-O bonds with non-uniform stretching vibrations in $[BO_3]$ units. The analytical findings indicate the predominant presence of $[BiO_6]$, $[BiO_3]$, and $[BiO_4]$ vibrations in the glasses. The Raman spectroscopy affirms the presence of distinct structural units, including BiO_3, BiO_6, BO_3, and BO_4. These findings provide a foundational basis for customizing glass compositions to meet specific technological requirements, encompassing applications in optics and radiation shielding.

Keywords: Density; Molar volume; OPD; FTIR; Raman

1 Introduction

Glasses attract significant interest owing to their diverse array of properties and applications, spanning non-linear optics, solar conductors, solid-state lasers, actuators, optoelectronic devices, and radiation shielding. The literature extensively covers different glass types, such as phosphate, tellurite, borate, germinate, silicate, fluoride, and borosilicate glasses. The bismuth borate system as a host is driven by its exceptional features, including a high refractive index, high density, broad transmission ranges from UV to IR, and a high dielectric constant[1]. Notably, bismuth oxide glasses, categorized as heavy metal oxide glasses (HMO) due to bismuth's classification as heavy metal, exhibit high polarizability. This characteristic renders them well-suited for applications in the domain of non-linear optics (NLO), ultrafast optical switches, and photonic devices. Despite these advantages, ongoing efforts are focused on improving the optical, electrical, mechanical, and thermal characteristics of bismuth-borate glasses[1-2].

Glasses enriched with heavy metal oxides, particularly those with a substantial concentration of Bi_2O_3, have garnered significant attention due to their diverse applications. These glasses containing high Bi_2O_3 content are employed as effective X-ray absorbers and play a crucial role in scintillation detectors utilized in high-energy physics. Additionally, bismuth borate glasses serve as excellent precursors for crafting ceramic superconductors. The presence of Bi_2O_3 in glasses results in a significantly high refractive index, a critical characteristic for sophisticated optical communication and processing equipment. Some researchers also reported the assumption that these glasses predominantly comprise highly distorted $[BiO_6]$ groups, as proposed by Bishay and Maghrabi[3]. In contrast, alternative viewpoints suggest that BiO_3 groups serve as the primary formers, with BiO_6 groups acting as modifiers. More recent literature postulates a coexistence of both BiO_3 and BiO_6 units in glasses containing Bi_2O_3, emphasizing that the proportion of each group depends upon various factors[3-4].

Over the last four decades, borate glass has emerged as a material of significant interest due to its promising mechanical and optical properties. These attributes have spurred exploration for potential applications in both industrial and medical fields. Borate glasses have a high density and highly hygroscopic nature, showcase beneficial features, including elevated mechanical strength, low phonon

*Corresponding author: (E-mail: meenakshi4phy@gmail.com)

energy, low melting point, and a high transparency. Research indicates that the presence of small quantities of alkali and alkaline elements as modifiers, along with lanthanides as dopants, enhances the properties of borate glasses[5]. Doping emerges as a key strategy for improvement, and numerous reports delve into the effects of various dopants and their properties[1].

This usage is primarily attributed to bismuth's non-toxic nature. Within the glass matrix, the inclusion of sodium oxide has notable effects on various physical properties including an elevation in density and refractive index, along with a reduction in both temperature and viscosity. Chromium oxide, among various transition metal ions, has piqued the interest of numerous researchers owing to its distinctive absorption and emission properties. Even in small concentrations within the glass network, this economically viable ion imparts colour to the glass and significantly influences its optical and dielectric properties[6]. The Cr^{3+} ion serves as a valuable tool for investigating the structure intricacies and local symmetries within developing glassy materials. Within glass phases, these ions inhabit distinct sites characterized by diverse field strengths, a result of positional variations and compositional disorder. Cr(III) ions also serve as probes in studies involving nanomaterials, existing in glasses with Cr^{3+} states featuring CrO_6 structural units[2]. Chromium oxide (Cr_2O_3) is employed in the form of a compound during the polishing (stropping) of knife edges, razors, optical devices, *etc*., on materials like leather, balsa or cloth. This compound often referred to as "green compound" and available in powder or wax form, plays a crucial role in such applications. Additionally, chromium oxide is utilized as a component in refractories due to its high melting point[7-8].

Borate glass has garnered attention for its promising mechanical and optical characteristics, making it a material of significant interest in recent decades. The incorporation of chromium oxide (Cr_2O_3), a transition metal oxide, into the composition can lead to glass suitable for applications in lasers and high-temperature sensors. Furthermore, literature surveys indicate that the introduction of specific oxides, such as Cr_2O_3, into the glass matrix significantly influences the structural properties of $(50\text{-}x)B_2O_3.40PbO.10Na_2O_2.xCr_2O_3$[5]. The primary objective of this research is to comprehensively examine the structural implications arising from the presence of chromium ions in multicomponent bismuth borate glasses. Consequently, glasses with the compositional formula $x.Cr_2O_3.(70\text{-}x)B_2O_3.18Bi_2O_3.12Na_2O$ are synthesized with varying amounts of chromium oxide. The synthesis procedure and physical properties have been thoroughly investigated and reported, with a focus on examining their variations.

2 Experimental procedure

Sodium bismuth borate glasses were subject to modification with varying amounts of chromium oxide, following the composition $x.Cr_2O_3.(70\text{-}x)B_2O_3.18Bi_2O_3.12Na_2O$, where x takes values of 0, 0.15, 0.25, 0.35, and 0.50 Wt% denoted as CRBBN1, CRBBN2, CRBBN3, CRBBN4, CRBBN5. In the synthesis process, Boron oxide (B_2O_3, 99.99%) was replaced with different weight percentage of chromium oxide (Cr_2O_3, 99.99%) and sodium oxide (Na_2CO_3, 99.99%), as outlined in Table 1. The synthesis method involved finely grinding and transferring the appropriate weights of chemicals into crucibles. These crucibles, containing the chemical mixtures, were subjected to an electrically maintained furnace at 1200K for the duration of 45 minutes. Subsequently, the resulting melt was pressed onto stainless-steel plates. The ensuing glass samples underwent additional 2-hour annealing process at 300 °C to alleviate stress[3]. The absence of any discernible peaks in the XRD patterns obtained with Cu-K_α(λ =1.5406A^o) radiation from a Philips X-Pert Pro diffractometer conclusively validated the amorphous nature of the glass samples. Highly precise density measurements (± 0.001 g/cm^3) conducted using the Archimedes principle with xylene provided additional confirmation of the amorphous character of the synthesized glasses.

Table. 1 — Chemical composition of CRBBN glass batch in mol%

		The ratio of each component's mol %			
Glass labelled	Composition X values	Cr_2O_3	B_2O_3	Bi_2O_3	Na_2CO_3
CRBBN1	0	0	70	18	12
CRBBN2	0.15	0.15	69.85	18	12
CRBBN3	0.25	0.25	69.75	18	12
CRBBN4	0.35	0.35	69.65	18	12
CRBBN5	0.50	0.50	69.50	18	12

3 Experimental Results and Interpretations

3.1 XRD Analysis

To obtain information about the structural characteristics of the prepared samples, we conducted powder X-ray diffraction (XRD) analysis in the range of 10° to 80°, as illustrated in Fig. 1. This analysis offers insights into whether the samples possess a crystalline or amorphous nature. All prepared samples exhibit broad peaks at around 25° and 45°. The shift in the position of broad humps appear to indicate the structural changes with doping of Cr_2O_3. The absence of sharp peaks in the XRD patterns dismisses the possibility of long-range periodic arrangement or crystalline nature in the prepared samples, indicating instead a short-range order. These broad peaks in the XRD patterns are indicative of short-range order, further confirming the amorphous or glassy nature of the prepared samples Harita *et. al*[1-5,9].

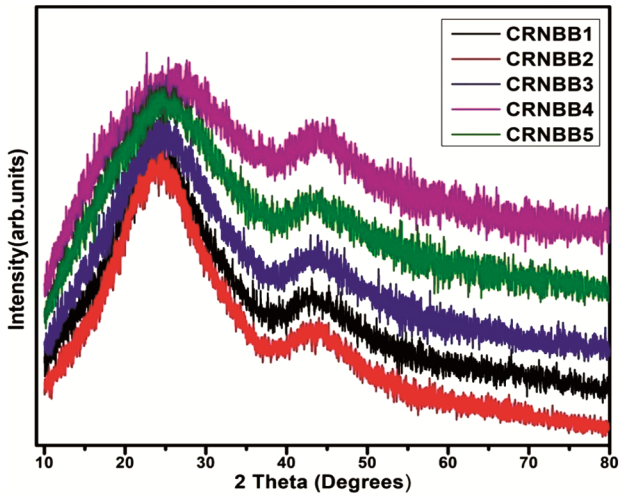

Fig. 1 — Illustrating XRDpatterns of quenched samples with different contents of Chromium oxide.

3.2 Physical Parameters of Glass Composition

Density is a parameter for investigating structural alterations within the glass system. The given formula is utilized to calculate the density of the glass samples.

$$[\rho = \frac{W_a \times J_{di}}{W_a - W_{di}}] \quad \text{...(1)}$$

ρ represents the Density of the glass specimen.

The provided formula (formula can be inserted if needed) utilizes density to assess changes in the glass structure. It relies on three key measurements:

- W_a: The weight of the glass specimen in air, reflecting its overall mass.
- W_{di}: The weight of the specimen when submerged in a liquid (usually water), representing the combined gravity of the glass and the displaced liquid.
- (W_a - W_{di}): The difference between the two weights, which signifies the buoyancy force acting on the glass due to the displaced liquid volume.

J_{di} is the density of de-ionized water utilized; Table 2 displays the calculated density values (ρ), which demonstrate structural alterations[10]. An electronic balance (Contech) was used to take each measurement. Density which denotes how compact

Table. 2 — List of variationsin physical parameters Density (ρ), Molar volume (V_M), crystalline volume, ionicity, ion concentration, chromium oxide interionic distance, and polaron radii of the glass systemx.Cr_2O_3.(70-x)B_2O_3.18Bi_2O_3.12Na_2O

Sample label	CRBBN1	CRBBN2	CRBBN3	CRBBN4	CRBBN5
Parameters	x = 0	x = 0.15	x = 0.25	x = 0.35	x = 0.50
Density (ρ) (g/cm^3)	3.822	3.871	3.903	3.944	4.009
(M_w)Average molecular weight (g/mol)	140.044	140.168	140.250	140.332	140.456
(V_M)Molar volume (cm^3 /mol)	36.63	36.20	35.929	35.572	35.035
(OPD) Oxygen packing density (mol/L)	75.34	76.227	76.818	77.588	78.777
Ionic concentration (N)$10^{20}/cm^3$	13.5	13.8	14	14.3	14.7
Bond density ($n_b \times 10^{24} m^{-3}$)	9.86	9.98	10.1	10.20	10.3
Electronegativity Difference (Δx)	1.606	1.607	1.607	1.607	1.608
Bond Ionicity (I_b)	0.4756	0.4758	0.4759	0.4760	0.4762
$R_i \times 10^{-8}(cm^{-1})$	9.06	8.99	8.94	8.88	8.79
$R_p \times 10^{-8}(cm^{-1})$	3.65	3.62	3.60	3.58	3.54
$F \times 10^{15}(cm^{-2})$	3.90	3.96	4.01	4.06	4.14

the glass network is can be correlated with structural stability. According to the relationship between molar volume (V_M) and density (ρ), the values of molar volume (V_M) gradually decrease as the number of doping increases.

$$V_M = \frac{M_W}{\rho} \quad ...(2)$$

M_w is derived from the below formula.

$$M_W = \sum X_i m_i \quad ...(3)$$

In the provided equation, X_i denotes the fraction of moles assigned to the i^{th} component, and M_i represents the total molecular mass of the i^{th} component. The density (ρ) and molecular volume (V_M) of the investigated glass sample are composition-dependent. Utilizing the molecular volume of glasses is a recommended approach to elucidate network structure and arrangement of building units. Which addresses the oxygen network's spatial organization Therefore, by analysing these parameters M_w and V_M, researchers can unlock the secrets of network organization and tailor the composition and properties of glasses for diverse applications[20].

The Oxygen packing density (OPD) of a material can be calculated based on the provided mathematical expression.

$$OPD = \frac{\rho \times n \times 1000}{M_W} \quad ...(4)$$

ρ represents the Density, while "n" indicates the quantity of oxygen atoms within a single unit[10]. The sample's Molecular Weight is denoted as M_w. A higher OPD indicates a tighter packing of oxygen atoms, potentially implying stronger bonds within the network and a more compact structure. Conversely, a lower OPD suggests a looser arrangement of oxygen atoms, possibly due to the presence of voids or weaker bonds[10].

The concept of "crystalline volume," which is stated as the space occupied by crystalline phases within a glass network, is.

$$V_C = \sum X_i V_i \quad ...(5)$$

Here V_c corresponds to the molar volume of the ith species in the crystalline phase, with specific values tabulated in Table 2.

(N) The ion concentration of glass samples means the number of ions present per cubic centimetre is determined using the below formula[30].

$$N = \frac{\rho \times N_A \times n \times X_{Cd}}{M_{Cd}} \quad ...(6)$$

"X" denotes the mole fraction, ρ denotes the density, N_A corresponds to Avogadro's number, and M_w represents the average molecular weight of each sample.

Bond density calculated using,

$$n_b = \frac{N_A}{v_M} \Sigma(n_C x_i) \quad ...(7)$$

N_A denotes Avogadro's number, V_M denotes the molar volume, and n_c is the coordination number of cations for Bi+, Cd^+, B^+ is 6,6,4,6[11-13,29].

The electro negativity difference is calculated[29],

$$\Delta X = \Sigma x_i \Delta x_i \quad ...(8)$$

The calculation of electro negativity disparity ($\Delta X_i = X_a - X_c$), representing the difference in electro negativity (X_i) among various oxide constituents within the glass composition, is derived from an exhaustive analysis of pertinent literature. The recorded electro negativity values for specific pairs, including Cr-O, Bi-O, and Na-O, B-O, stand at 1.78, 1.42, 2.51, and 1.5, respectively, as documented in the literature. Here, 'X_a' and 'X_c' denote the difference in electro negativity between the anion and cation respectively[10-13].

3.2.1 Bond-ionicity

The ionic character of a bond can be influenced by factors including the electro negativity difference between the involved atoms, the size of the atoms, and the nature of the elements. A higher electronegativity difference and smaller atomic sizes tend to increase the ionic character of a bond, represented by bond ionicity, which is determined by utilizing values of electro negativity difference as derived from the calculated equation.

$$I_b = 1 - \exp(-0.25(\Delta x)^2) \quad ...(9)$$

Calculated values are presented in Table 2.

Finally, (R_i) interionic radii of the glass specimens were accomplished by utilizing the value of "N".

$$R_i = \left(\frac{1}{N}\right)^{1/3} \quad ...(10)$$

The polaron radius (R_p), which represents the size of a localized electronic defect. This value is calculated using the formula provided in the equation, incorporating the values of "n". Observing the

decrease in both R_i (ionic radius) and R_p as the chromium oxide content increases. This reduction signifies a shorter Cr-O distance. Interpreting the shorter Cr-O distance as indicative of stronger Cr-O bonds, ultimately contributing to a stronger field strength (F)[14]. To understand the spatial arrangement and bond strength of chromium ions within the glass systems, calculated the chromium yield field strength (F). This calculation involves:

$$R_p = \frac{1}{2}\left(\frac{\pi}{6N}\right)^{1/3} \quad ...(11)$$

$$F = \frac{Z}{{R_p}^2} \quad ...(12)$$

Density and molar volume measurements for various glass compositions were performed at room temperature using the Archimedes principle. Fig. 2(a,b) presents the compositional dependence of these properties, while Fig. 3(a,b) explore their other physical variations specifically for increasing chromium oxide concentrations (x = 0, 0.15, 0.25, 0.35, and 0.50 mol %) across all glass systems. Particularly, a consistent non-linear decrease in molar volume is observed within all glasses, counteracting the trend exhibited by density Fig. 2(a).

Within these glass systems, an intriguing observation emerges density increases non-linearly (from 3.82 to 4.009 g/cc) with the augmentation of chromium oxide[6]. This finding, supported by the data presented in Table 2.The escalation in density linked to chromium oxide content can be ascribed to the incorporation of chromium ions in the interstitial spaces within the glass network. As chromium oxide (Cr_2O_3) was gradually added to the glass composition, its OPD and ionic concentration of chromium ions

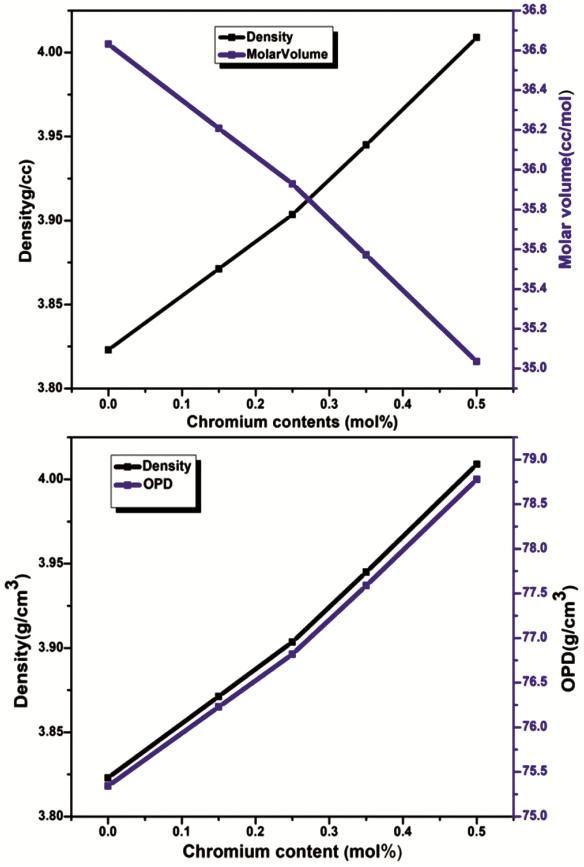

Fig. 2 — (a) The system's density (ρ) and molar volume (V_m) exhibit compositional dependence $x.Cr_2O_3.(70\text{-}x)B_2O_3.18Bi_2O_3.12Na_2O$, where x varies (0, 0.15, 0.25, 0.35, 0.50 mol %) (b) Dependency of Density (ρ) and OPD , $inx.Cr_2O_3.(70\text{-}x)B_2O_3.18Bi_2O_3.12Na_2O$ glass system, with the varies value of x(0, 0.15, 0.25, 0.35, 0.50 mol %)

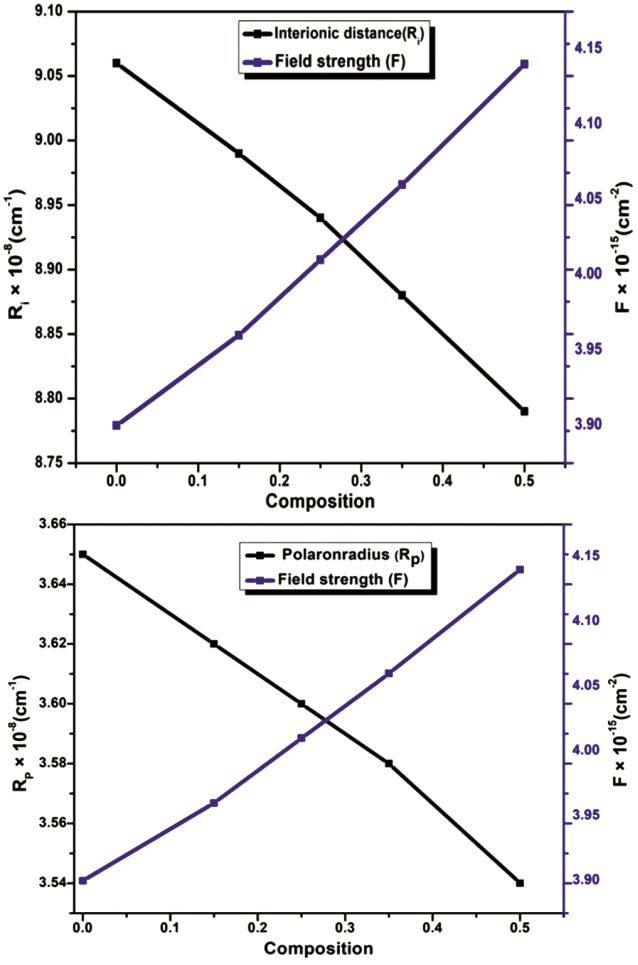

Fig. 3 —(a) Variation of chromium oxide interionic distance (R_i) and chromium yield field strength (F) for $x.Cr_2O_3.(70\text{-}x)B_2O_3.18Bi_2O_3.12Na_2O$ glass system (b) chromium oxide polaron radius (R_p), chromium yield field strength (F) $x.Cr_2O_3.(70\text{-}x)B_2O_3.18Bi_2O_3.12Na_2O$ glass system with variation of concentration (x = 0, 0.15, 0.25,0.35, 0.50 mol%)

steadily increased from (75.34 to78.77), (1.35 to 1.47) Fig. 2(b). This rise can be attributed to the replacement of lighter boron atoms (relative atomic mass 10.811u) with heavier chromium atoms (51.996 u). Evidently, while density increased, the calculated molar volume showed a concurrent decrease with the increasing mol % content of Cr_2O_3. This contrasting behaviour serves as a strong indicator for the increasing compactness of the glasses. The increasing Cr_2O_3 content also triggered a notable rise in the field strength (F) of Cr-O bonds escalating from 1.6×10^{15} to 6.7×10^{15} cm^{-2}, Fig. 3(a,b). This stronger interaction between oxygen ions led to a reduction in their intrinsic spacing (R_i), effectively shortening the bond length from 9.056 to 8.79 Å. This reduction essentially translates to a higher bond stretching force constant, ultimately decreasing the molar volume and, in turn, boosting the glass density. The result is a denser glass matrix with enhanced properties.

Furthermore, decreasing polaron radius (3.65 → 3.54 × 10^{-8} cm^{-1}) with Cr_2O_3 addition highlights increased polarizability and network compactness[14]. The positive ΔV value further corroborates the glassy nature of the analysed composition. Higher EN(Electronegativity) difference leads to more polar covalent bonds with a significant ionic character. These bonds are stronger and more directional, resulting in a more rigid and chemically resistant glass and lower EN difference leads to more **non-polar covalent bonds,** characterized by a more evenly sharing of electrons between atoms. Such bonds exhibit lower strength and less directional, resulting in a more flexible and potentially more reactive glass. Glasses containing alkali metals (Li, Na, and K) with lower EN differences can exhibit higher thermal expansion coefficients and lower chemical resistance. Using the measured density (ρ) and calculated average molecular weight (M), we were able to quantify several crucial physical parameters of the material, including molar volume, transition metal ion concentration (N_i), and metal ion separation (R_i). These parameters provide valuable insights into the material's structure, composition, and properties[10-14].

4 Structural investigations and Interpretations

4.1 FTIR Spectroscopy: Elucidating Molecular Structures and Chemical bonds

Samples were analysed by FTIR in this approach, which involves obtaining an infrared spectrum through the absorption or emission of solids, liquids, or gases, is the most widely used method in the field of infrared spectroscopy.

FTIR spectra were utilized to identify the structural components and chemical bonds of the materials at room temperature. FTIR spectroscopic techniques were employed to gain insight into the structural changes in local arrangements within both glass and glass ceramics. Borate glasses are a good case to demonstrate the effectiveness of IR spectroscopy as compared to other glass systems[9]. In the measurements of spectra, all vibrational bands appear above 500 cm^{-1} because boron has a small mass as we compare it to other glass-forming elements. FTIR spectroscopy proves to be a robust tool for elucidating the structural properties of oxide glasses, especially within the $x.Cr_2O_3.(70\text{-}x)B_2O_3.18Bi_2O_3.12Na_2O$ glass series. This encompasses a range of mole percentages spanning from 0 to 0.50% and is observed within the spectral range spanning from 400 to 4000 cm^{-1}, as depicted in Fig. 4. The intricate network of chromium sodium borate glasses is elegantly unveiled by analysing their FTIR spectra. These spectra reveal three distinct absorption bands, each offering a window into the complex interplay of atoms and bonds within the material.

Three distinct absorption regions, spanning are 530-840cm^{-1}, 840-1150 cm^{-1} and 1150-1600 cm^{-1} are observed in the FTIR spectra of CRBBN glasses. These regions hold valuable clues about the vibrational modes present in the glass network. The first and third bandsB-O-B bond movements in the triangular [BO_3] units coupled with the three oxygen atoms (both bridging and non-bridging types) are

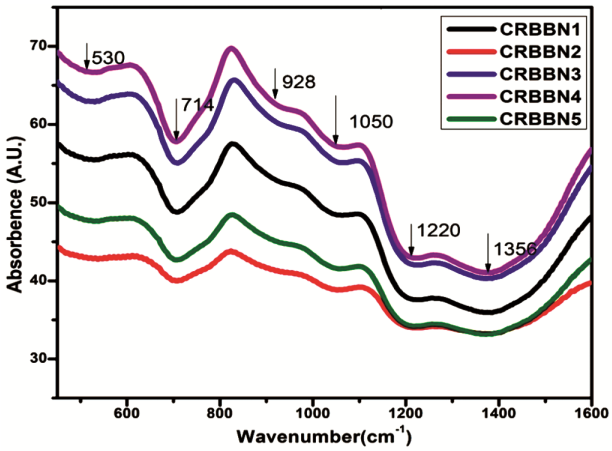

Fig. 4 — FTIR spectra for $(CRBBN)x.Cr_2O_3.(70\text{-}x)B_2O_3.18Bi_2O_3.12Na_2O$ glass system with varying concentration (x = 0, 0.15, 0.25,0.35, 0.50 mol%)

responsible for the first and third absorption domains respectively.

- A band in the range of ~530-840 cm^{-1} arises from the bending vibrations of various borate groups[31].
- A medium absorption band spanning ~840-1150 cm^{-1} is associated with the stretching of tetrahedral BO_4 units[10,31].
- An absorption band spanning ~1150-1600 cm^{-1} is associated with the stretching of tetrahedral BO_3 units[11].

The coexistence of BiO with B_2O can impact the glass matrix by altering the structural groups from BO_3 to BO_4. Additionally, it contributes to the structure as a pyramidal group BiO_3 and introduces non-bridging oxygen. In the spectra the first band moves in direction of higher wave number 840cm^{-1} by increasing chromium content or by decreasing borate ions which attributed the stretching and bending vibrations in NBO with [BO_3] units. This band is created by Bi-O linkages in the [BiO_6] octahedral. A band observed at 530 cm^{-1} is presumed to arise from Bi–O linkages within the BiO_6 octahedral units[32,33]. The position of this band may undergo a shift to a higher or lower wave number, influenced by the degree of distortion introduced by the type of transition ions added[3-4]. The band observed at 708-714 cm^{-1} is associated with super structural borate units and can exhibit variations in intensity due to factors such as alterations in the configuration of certain borate arrangements relative to boron 4 coordination, the borate anomaly, or the type of introduced transition metal (TM) ions (Dimitrov *et al.*, 1994). According to Baia *et al.* (2003), bismuth borate has three possible groups to be found in the network either as [BiO_6] or both [BiO_6] and [BiO_3] or only as [BiO_3] pyramidal units[4,15-16]. In this band, a noticed shift towards a higher wave number is prompted by the increase in the degree of distortions. When highly distorted [BiO_6] polyhedral local symmetry changes, the band shifts from a lower to a greater wave number, with a decrease in [B_2O_3] content[17]. At the second region [840-1150cm^{-1}] increase in extending vibratory intensity with the increasing Chromium content creates non-bridging oxygen in tetrahedral [BO_4] units[33]. The 906–935cm^{-1} band, it stems from stretching movements of B–O bonds within BO_4 tetrahedral. As the concentration of Cr increases further, there is a notable shift in peaks and shoulders towards the 1600 cm^{-1}range. Within the 1038–1400 cm^{-1} range, another band arises as a stretching vibration of Bi-O bonds in BiO_6 octahedral1[8,33-35]. Consequently, this caused the extension of the B-O linking oxygen with a different group such as boroxol rings along with triangular [BO_4] units present in Tri, tetra, and Penta borate groups. The alteration indicates the extension of these bonds, and it is attributed to a progressive rise in Cr concentration. This effect is particularly noticeable in the interaction between Cr and mentioned structural units, influencing their vibrational behaviour[10-18]. Peaks resolved in deconvoluted spectra in Fig. 5 and Table 3 for the given composition, and we can predict some parameters such as amplitude (A), X_c denotes the position of the peak, and W denotes the width of 1/2 maxima. The presence of peaks within the 500-600 cm^{-1} ranges is ascribed to vibrations originating from Bi-O bonds within the respective octahedral units. These vibrations occur because of the bending of trigonal units. The deconvoluted data peaks at the 605–740 cm^{-1} range can be associated with diverse phenomena arising from the B–O–B bond within the borate glass network. The borate glass network will exhibit BO_3-BO_4 vibration bending above this range. The vibrations of the [BO_4] units may have caused the peak at 714 cm^{-1}. The peaks within the 800-1000 cm^{-1} range are associated with symmetrical stretching vibrations, primarily stemming from Bi-O bonds and these vibrations are a consequence of the presence of trigonal [BiO_3] units. These vibrations overlap with different configurations of [BO_4] units within the glass structure. Additionally, there's a peak at 1191 cm^{-1}, which corresponds to the asymmetric vibrations and stretching arising from Bi-O-Bi bonds within the trigonal unit [BO_3]. These [BO_3] units are typically part ofpyro and ortho-borate groups. Furthermore, the presence of peaks spanning from 1200-1300 cm^{-1} indicates B-O bond stretching vibration in the trigonal

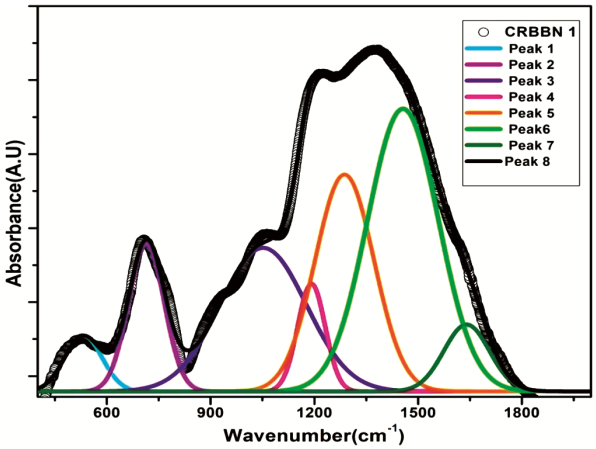

Fig. 5 — Gaussian Deconvoluted infrared spectra of CRBBN1

Table. 3 — IR wave number assignment of different vibrational modes for $x.Cr_2O_3.(70-x)B_2O_3.18Bi_2O_3.12Na_2O$ glass system

Peak (cm^{-1})	IR spectra Investigations	Reference
450	The band positioned is due to the metal cationNa^+, Cr^+vibrations.	
540-600	The presence of structural units [BO_3] and [BO_4], overlaps with the Bi-O bonds in [BO_6] units. The bands in the vicinity are ascribed to the vibrations of Bi–O bonds within BiO_6 units.	[11][12][13][9]
714-900	The observed bands correspond to symmetric stretching of the Bi-O linkages within [BiO_3] units, and bending vibrations attributed to BO_3-BO_4linkages.Additional stretching and bending involve various elements in glass composition.	[11][19][6]
928-1050	The identified spectral feature is ascribed to the B–O stretching vibration of BO_4 units, shared among different borate groups such as di-, tri-, and penta-borate groups. This observation provides evidence for the existence of bothboron oxide and bismuth oxide units within the intricate structure of the glass network.	
1040-1150	Symmetrical stretching vibrations originating from [BO_3], and [BO_4] units. Polyhedral [BiO_3] has a distinct vibrational band. Penta-, tetra-, and Tri-borate groups are responsible for B-O stretching movements. In [BO_4] modes of di-borate groups, B-O stretching movements.	[6][19][13]
1220-1300	The observed spectral bands correspond to the B-O linkage asymmetric stretching movements in [BO_3] units within ortho- and pyro-borate groups.	
1356-1400	Non-uniform Stretching vibration of B-O linkage in BO_3 units from rings (boroxol). Peaks in this range reveal the presence of the structure of rings (boroxol) and triangular Units.	[6][10][13][19]
1401-1540	The detected vibrational modes are associated with the Bi-O linkages in [BiO_6] and [BiO_3] units, along with B-O bond stretching vibrations within [BO_3] units derived from distinct types of borate groups.	[6][19]
1500-1670	Vibration of OH bonds.	[11]

unit [BO_3] originated from rings (boroxol). These vibrations are characteristics of the structural arrangements within rings (boroxol) in the material [3,12-13]. The band located at 1330–1540 cm^{-1}, designated for metaborate superstructure units or pyborate, undergoes wavelength shift to lower values in the presence of Cr or Fe ions[4].

Moreover, attenuated bands in the FTIR spectra may be indicative of vibrational modes pertaining to additional glass components, such as sodium oxide (Na_2O). This provides a nuanced understanding of the vibrational dynamics within the glass network 9-13 (Table 3).

As illustrated in Fig. 5, CRBBN1, the peak at 532 cm^{-1}, typically linked to the bending vibration attributed to the Bi-O-Bi linkages within bismuth oxide clusters (in the absence of chromium doping), exhibits similarities to the B–O stretching observed at 714 cm^{-1}. The vibration at 714 cm^{-1} is specifically associated with Bi–O-Bi, indicating bending vibrations within the bismuth borate network. The vibration at 1052 cm^{-1} associated with symmetrical vibrations of Bi–O-Bi, while the one at 1191 cm^{-1} is linked to the non-uniform stretching vibrations in Bi–O-Bi. The peak at 1287 cm^{-1} corresponds to the uniform vibration of B-O bonding, while the peak at 1456 cm^{-1} is linked to the B-O-B bending movement within borate structures. Additionally, the presence of the peak at 1640 cm^{-1} resembling the stretching movement of O–H bonds in water molecules or hydroxyl groups (Table 4)[11]. Is notable in the subsequent samples CRBBN2, CRBBN3, CRBBN4, CRBBN5 around 540 cm^{-1}. Furthermore, the range between 505 and 750 cm^{-1} encompasses distinctive bending movements correlated with Bi-O-Bi bonds within bismuth oxide clusters, confirming the structural consistency across diverse compositions[20]. In the 1050 cm^{-1} range, distinct vibrations linked to Bi–O-Bi bonds become evident, featuring symmetric vibrations at 1191 cm^{-1} and asymmetric stretching vibrations around 1287 cm^{-1}. The 1400 cm^{-1} range highlights B-O-B bending movements, indicating the prevalence of borate structures across diverse glass compositions. Concurrently, the consistent observation of stretching movements related to O–H linkages at 1600 cm^{-1} emphasizes the widespread occurrence of these vibrational features. The identified peaks underscore the uniform structural elements present in chromium oxide-doped bismuth-borate glasses, presenting avenues for customizing material properties and exploring novel applications in materials science[20-22,9-13]. A progressive reduction in peak intensity is noted with the diminishing concentration of bismuth. New peaks are present as the chromium oxide concentration increase from CRBBN1 to CRBBN5.

Table. 4 — Various parameters were derived from the deconvoluted FTIR absorption spectrum, where X_c, A, and W denote the peak position, relative area, and full width at half maximum of the deconvoluted spectra of $x.Cr_2O_3.(70\text{-}x)B_2O_3.18Bi_2O_3.12Na_2O$

Peak	CRBBN1			CRBBN2			CRBBN3			CRBBN4			CRBBN5		
	X_C cm^{-1}	A a.u.	W cm^{-1}	X_C cm^{-1}	A a.u.	W cm^{-1}	X_C cm^{-1}	A a.u.	W cm^{-1}	X_C cm^{-1}	A a.u.	W cm^{-1}	X_C cm^{-1}	A a.u.	W cm^{-1}
1.	532	510	108.69	541	196	92.59	505	346	83.811	712	1492	95.86	710	749.16	95.77
2.	714	1292	103.18	714	549	103.39	740	1506	122.41	534	491	99.03	1068	2605.15	409.42
3.	1052	3209	249.167	907	114.58	71.54	972	982	128	1020	2783	212.45	1659	718.95	318.31
4.	1191	724	79.428	1114	243.43	64.91	1469	6146	239.69	1199	1095	87.17	1368	737.16	324.57
5.	1287	3128	170.36	1191	3551	308.55	1231	6270	236.48	1352	9523	266.70	1319	581.92	138.02
6.	1456	4913	205.27	1456	2441	248.036				1556	2337	186.98			
7.	1640	2319	132.141 2												
Functional groups	Stretching of B-O bond Bi–O-Bi Bond with asymmetric Stretching Stretching of Bi–O-Bi bond Bending of Bi–O bond Bending and stretching of B-O bond			B-O-B Bending Bending of Bi–O-Bi bond Bi–O-Bi withsymmetric Stretching Vibration Bi–O-Bi with Non-uniform Stretching movement. B-O-B bond withbending vibration			Stretching of B–O bond Stretching of Bi-O bond Bi–O-Bi bond with asymmetric stretching Bi–O-Bi bondstretching. B-O bond Bending			Bending vibration B-O-B Stretching Vibration of Bi–O-Bi bond Bi–O-Bi bond withSymmetric Stretching Vibration Bending Vibration of Bi–O-Bi bond Stretching Vibration of B-O bond Bi–O-Bi bond with asymmetric stretching vibration			Stretching of B–O bond Stretching Vibration of Bi–O-Bi bond Bi–O-Bi bond with asymmetric stretching Bi–O-Bi bond stretching. B-O bond bending		

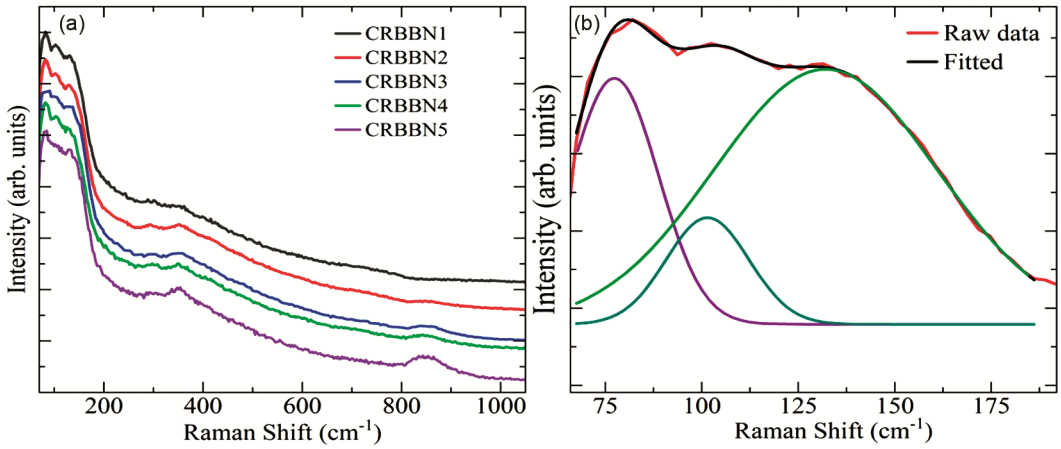

Fig. 6 — (a) Raman spectra for composition CRBBN $x.Cr_2O_3.(70\text{-}x)B_2O_3.18Bi_2O_3.12Na_2O$ glass system with varying concentration (x = 0, 0.15, 0.25,0.35, 0.50 mol%) (b) Raman deconvoluted spectra for sample CRBBN1

4.2 RamanInvestigation: Chemical analysis using Raman scattering

The spectra display the deconvoluted data along with corresponding peaks Fig. 6(a) as listed in Table 4, and Table 5. Peak observed within the range of 65 to 88 cm^{-1} is indicative of vibrational modes associated with bismuth ions of E_g symmetry. The observed peaks in data of all samples at a position between 133 to 160 cm^{-1} may originate from heavy metal (Bi^{3+}) within the [BiO_6], and [BiO_3] octahedral vibrations. This implies that the vibrational modes correspond to the movement of the bismuth ion[10]. The presence of bending vibrations in tetrahedral units is indicated by the Raman peaks observed within the spectral range of 150-251 cm^{-1}[11,23]. As the concentration increase of chromium a peak is ranging 295 cm^{-1} is highlighted due to vibration mode of bismuth ion.

Stretching vibrations of the Bi-O bond characterized by bismuth ion within the frequency

Table. 5 — Allocating Raman wavenumber to different vibrational modes for $x.Cr_2O_3.(70\text{-}x)B_2O_3.18Bi_2O_3.12\ Na_2O$ glass system

Raman shift (cm^{-1})	Raman spectroscopic characterization
65-88	Vibrational modes exhibited by bismuth ions of the E_g symmetry[6].
133-160	Bi^{3+} ion of [BiO_6], [BiO_3] octahedral unit caused oscillation[10,26].
300-364	Vibrational modes of [BO_3] and [BO_4] units.
349-383	Uniform stretching movements of Bi-O bond of bismuth ion[10]. Bi-O-Bi bonding is present in [BiO_3], and [BiO_6] modes, which generate vibration[10].
410-662	Metaborate groups in ring structure cause Bi-O bond stretching movements in [BiO_6] units. The Correlation of Cr^{+3}modes also result in the B-O bonds bending[10,11].
621-656	In Tetra-Borate groups of [BO_3] units, there are vibrational modes within the bonds such as B-O-B and B-O[10].
730-856	The stretching vibrations of the B-O bond in orthoborate arise from the BO_4 pyramidal modes .
879-936	Pentaborate groups presents[6].
981-1015	Di-borate groups present.
1200-1299	Formation of pyro borate modesassociated with thenon-uniform stretching of B-O-B bridges in B_2O_3.
1300-1400	OH Groups Present.

Table. 6 — Various parameters were derived from the deconvoluted RAMAN absorption spectrum, where x_c, A, and W denote the peak position, relative area, and full width at half maximum of the deconvoluted spectra of $x.Cr_2O_3.(70\text{-}x)B_2O_3.18Bi_2O_3.12Na_2O$

Peak	CRBBN1			CRBBN2			CRBBN3			CRBBN4			CRBBN5		
	X_c (cm^{-1})	A a.u.	W (cm^{-1})	X_C (cm^{-1})	A a.u.	W (cm^{-1})	X_C (cm^{-1})	A a.u.	W (cm^{-1})	X_C (cm^{-1})	A a.u.	W (cm^{-1})	X_C (cm^{-1})	A a.u.	W (cm^{-1})
1	98	44819	48.01	80	2338	23.44	82	4.85	6.36	80	1366	23.80	73	401	15.48
2	144	1.11	26.9	81	2722	25.0	115	4976	75.83	123	369	59.09	92	731	28.19
3	152	2797	48.0	124	902	71.35	127	5856	1823	150	468	47.89	132	169	53.1
4	247	3528	158.9	128	850	67.26	128	542	86.09	201	211	116.59	192	100	86.4
5	416	5745	278.28	224	1477	273	310	877	347	228	2.12	167	460	147	211
6				264	863	204	323	6523	300	230	1.99	160	695	290	165
				421	1770	433				289	656	18	850	142	59.50
				681	867	166.6				377	668	298.1			
possible fuctional groups	O-Bi–O bending Bi-O stretching Bi–O-Bi bending			O-B–O bending Bi-O stretching BI–O-Bi bending B-O-B bending			B–O bending Bi-O stretching Bi–O-Bi bending O-Bi-O bending			O-Bi–O bending Bi-O stretching Bi–O-Bi bending O-Bi-O bending			O-Bi–O bending Bi-O stretching Bi–O-Bi bending B-O-B bending		

range of 300 to 364 cm^{-1}. Vibrational forms attributed to [BiO_6], and [BiO_3] unit of glassy material are responsible for peaks appearing in the range 177 to 383 cm^{-1}. Peaks positioned from 349 to 383cm^{-1} may correspond to vibrational forms of the Bi-O-Bi band within the [BiO_6] octahedral unit. The peak in this range provides information about ring structure and modes related to aromatic and heteroaromatic compounds. The vibrational modes arising from the stretching of Bi-O within the [BiO_6], [BO_4] unit, along with the existence of metaborate groups forming a ring-type structure, give rise to the observed vibrations in the range of 500 to 600cm^{-1}[11]. The existence of borate groups of [BO_3] unit can be used to explain the peaks falling within the spectral range of 750 to 856 cm^{-1}[28]. The transition from higher to lower wave numbers within the range of 621-651 cm^{-1} occurs up to CRBBN2 and subsequently shifts for CRBBN4 and CRBBN5, indicating the influence of pentaborate groups[11-13]. The spectral band seen within the range (730-756) cm^{-1}, indicates the breathing vibrations associated with a six-member ring having a single tetrahedral unit[24]. A shift to a lower wavenumber with a simultaneous decrease in intensity is noted upon the addition of chromium oxide content from CRBBN1 to CRBBN5. The rings observed in di-triborate, diborate, and pentaborate forms may undergo disruption, leading to a decrease in the intensity of this group. This suggests the transformation of some rings into chain and ring-type metaborate groups[25]. The peak corresponds to the vibrational stretching of B-O bonds can be seen in the deconvoluted spectra at the position between 1300 cm^{-1} and 1344 cm^{-1}. This region includes vibrational modes with N-O and C-R bonds. It reveals information about double and triple bonds in

molecules. These bonds encompass pyroborate groups that are integral to the interlinkedstructure of boron and oxygen. Apparent peaks result from vibrational modes stemming from B-O bonding within the [BO_3], [BO_4] unit present in glassy material. As the content of Chromiumoxide increases, the intensity of these bonds increases[9-13].

The identified Raman peaks in bismuth glasses offer valuable information about the vibrational modes associated with structural units within the glass matrix. The units identified exhibit specific vibrational characteristics: including, Bi–O, Bi–O-Bi stretching vibrations, and O-Bi-O binding vibrations[13,24,25]. In CRBBN1, the spectrum revealed peaks at 92 cm^{-1}, 127 cm^{-1}, 169 cm^{-1}, and 241 cm^{-1}, as illustrated in Fig. 6(b). These peaks were associated with the bending vibrations of O-Bi–O, stretching vibrations of Bi-O, and bending vibrations (O-Bi–O, Bi–O-Bi) within the glass system[13]. In, CRBBN2, an additional peak at point 295cm^{-1} associated with bending vibrations of O-Bi–O, while peaks at 120 cm^{-1}, 172 cm^{-1}, 311 cm^{-1} and 469 cm^{-1}correspond to Bi-O stretching vibrations. The presence of B_2O_3 as a network modifier is suggested by the observed peak at 469 cm^{-1}, indicating B-O-B bending or stretching vibrations. The Raman spectra of bismuth borate glasses exhibit stretching vibrations. The all samples show that the detected peaks appeared at last as the concentration of chromium oxide is increased and the behaviour of bends are reported different. The examination of FTIR spectroscopy and Raman data of the current glass system reveals the presence of [BiO_3], [BiO_6], and [BO_4] structural units in composition. Furthermore, the study reveals the existence of both symmetric and asymmetric stretching vibrations of BO_4. As the content of chromium oxide increases, symmetric vibrations tend to dominate. This occurrence may be ascribed to the substitution of larger bismuth oxide molecules with smaller chromium oxide molecules[6-13,27].

5 Conclusion

We have investigated the influence of Cr_2O_3 on the structural and physical characteristics of chromium oxide bismuth borate glasses represented by the formula $x.Cr_2O_3.(70\text{-}x)B_2O_3.18Bi_2O_3.12Na_2O$ (x=0, 0.15, 0.25, 0.35, 0.50 wt%). There is an increase in the density of the synthesized samples with an increase in the Cr_2O_3 content. The XRD analysis confirms the amorphous nature of the glasses, indicating a uniform glass network without crystalline phases. Structural investigations conducted through FTIR and Raman spectroscopy affirm the presence of distinct structural units, including BiO_3, BiO_6, BO_3, and BO_4. The FTIR spectroscopy confirms the empirical presence of [BiO_6], [BiO_3], and [Cr^{3+}] structural elements within the glass matrix. Additionally, the spectra reveal vibrational modes associated with metal cation units (Cr^{3+} and Na^{2+}) and Bi–O bonds within the BiO_3 units. An increase in B_2O_3 content correlates with heightened density, reduced molar volume, and consequential changes in ionic concentration, collectively shaping the comprehensive composition and characteristics of the glass. This renders it potentially suitable for various applications across diverse technological domains. The thorough exploration of Raman spectroscopy, aimed at delineating vibrational modes, is underscored by the precise identification of BiO_3 and BiO_6 vibrational modes. Deconvolution analyses were systematically performed on glass specimens featuring diverse concentrations of chromium and sodium, revealing intricate vibrational modes and peak shifts. The density (ρ) of the glass exhibits a substantial increase with the progressive escalation of chromium oxide content. Conversely, the consistent decline in molar volume (V_m) across the entire chromium oxide content range highlights intricate structural changes. These nuanced insights into the behaviour of bismuth borate glasses offer valuable perspectives for their applications in the intricate realms of optoelectronics and photonics.

Acknowledgement

The authors would like to thank [Baba Masthnath University, Rohtak, India] for their valuable support and assistance during this research.

Reference

1 Nagaraju R & Kumar K V, *Int J Mech Eng*, 7 (2022) 641.
2 Phani A V L, Srinivas B, Hameed A, Chary M N, Rao J L & Shareefuddin M D, *Chin J Phys*, 58 (2019) 303.
3 Batal F Hel, Marzouk M A & Ghan A M A, *J Mater Sci*, 46 (2011) 5140.
4 Sallam O I, Ezz-Eldin F M & Elalail N A, *Opt Quant Electron*, 52 (2020) 204.
5 Al-Buriahi M S, Alajerami Y S M, Abouhaswa A S, Alalawi A, Nutaro T & Tonguc B, *J Non-Cryst Sol*, 544 (2020) 120171.
6 Haritha L, Sekhar K C, Nagaraju R, Ramadevudu G, Sathe V G & Shareefuddi Md, *Chin Phys B*, 28 (2019) 038101.
7 Jiao M, Wua H, Lia Z, Laia F & Lia J, *J Asian Ceram Soc*, 9 (2021) 1320.
8 Othman A M, El-Fattah Z M A, Farouk M, Moneep A M & Hassan M A, *J Non-Cryst Sol*, 558 (2021) 120665.
9 Sharma V, Singh S P, Mudahar G S & Thind K S, *New J Glass Ceram*, 2 (2012) 128.
10 Thakur S, Thakur V, Kaur A A & Singh L L, *J Non-Cryst Sol*, 52 (2019) 60.

11 Pawaria S, Ahlawat J, Bala M, Dahiya S, Ohlan A, Punia R & Maan A S, *J Mol Struct*, 1270 (2022) 133836.
12 Nain D, Deepika, Babita & Meenakshi, *Silicon*, 16 (2024) 1329.
13 Nain D, Maan D, Ahlawat J & Meenakshi, *Silicon*, 16 (2024) 2205.
14 Wagh A, Raviprakash Y, Upadhyaya V & Kamath S D, *Spectrochim Acta Part A: Mol Biomol Spectr*, 151 (2015) 696.
15 Dimitriev Y & Michailovo V, *Int cong Glass Madrid*, 3 (1992) 293.
16 Baia L, Stefan R, Keifer W, Pop J & Simon S, *J Non-Cryst Sol*, 303 (2002) 379.
17 Dahiya M S, Meenakshi, Shankar A, Agarwal A & Khasa S, *J Alloy Comp*, 696 (2017) 688.
18 Alajerami Y S, Drabold D A, Mhreb M & Subedi K N, *J Appl Phys*, 127 (2020) 1.
19 Rejisha S R, Anjana P S, Gopakumar N & Santha N, *J Non-Cryst Sol*, 388 (2014) 68.
20 Punia R, Kundu R S, Hooda J, Dhankhar S, Dahiya S & Kishore N, *J Appl Phys*, 110 (2011) 33527.
21 Gautam C, Yadav A K & Singh A K, *ISRN Ceram*, 1 (2012) 428497.
22 Boda R, Sharfuddin M, Chary M N & Sayanna R, *Inorg Mater Today Proc*, 3 (2016) 1914.
23 Bala M, Pawaria S, Deopa N, Dahiya S, Ohlan A, Puni R & Maan A S, *J Mol Struct*, 1234 (2021) 130160.
24 Hivrekar M M, Sable D B, Solunke M B & Jadhav K M, *J Non-Cryst Sol*, 474 (2017) 58.
25 Meera B N & Ramakrishna J, *J Non Cryst Solids*, 159 (1993) 1.
26 Singh L, Thakur V, Punia R, Kundu R S & Singh A, *Sol State Sci*, 1 (2014) 64.
27 Aktas B, Yalcin S, Dogru K, Uzunoglu Z & Yilmaz D, *Radiat Phys Chem*, S0969 (2018) 30512.
28 Sangeetha G, Sekhar K C, Hameed A, Ramadevudu G, Chary M N & Shareefuddin M, *J Non Cryst Sol*, 563 (2021) 120784.
29 Abdel-Baki M, Abdel-Wahab F A & El-Diasty F, *J Appl Phys*, 111 (2012).
30 Bala M, Pawaria S, Deopa N, Dahiya S, Ohlan A, Punia R & Maan A S, *J Mol Struct*, 1234 (2021) 130160.
31 Abdelghany A M & Behairy A, *J Mater Res Technol*, 9 (2020) 10491.
32 Sumalatha B, Omkaram I, Rajavardhana R T & Raju L, *Phys B: Cond Matter*, 411 (2013) 99.
33 Girsova M, Goloina G, Kuilenko L & Antropova, *Glass Phys Chem*, 41 (2015) 93.
34 Chandrakiram G, Yadav A K & Singh A K, *ISRN Ceram*, 2012 (2012) 428497.
35 Rada S, Ristoiu T, Rada M, Coroiu I, Maties V & Rada C E S, Ristoiu T, Rada M, Coroiu I, Maties V & Culea E, *Mater Res Bullet*, 45 (2010) 69.